Environ Fluid Mech (2014) 14:173–200
DOI 10.1007/s10652-013-9287-2

ORIGINAL ARTICLE

Numerical modelling of horizontal sediment-laden jets

S. N. Chan · Ken W. Y. Lee · Joseph H. W. Lee

Received: 6 December 2012 / Accepted: 6 May 2013 / Published online: 18 May 2013
© Springer Science+Business Media Dordrecht 2013

Abstract Sediment-laden turbulent flows are commonly encountered in natural and engineered environments. It is well known that turbulence generates fluctuations to the particle motion, resulting in modulation of the particle settling velocity. A novel stochastic particle tracking model is developed to predict the particle settling out and deposition from a sediment-laden jet. Particle velocity fluctuations in the jet flow are modelled from a Lagrangian velocity autocorrelation function that incorporates the physical mechanism leading to a reduction of settling velocity. The model is first applied to study the settling velocity modulation in a homogeneous turbulence field. Consistent with basic experiments using grid-generated turbulence and computational fluid dynamics (CFD) calculations, the model predicts that the apparent settling velocity can be reduced by as much as 30 % of the stillwater settling velocity. Using analytical solution for the jet mean flow and semi-empirical RMS turbulent velocity fluctuation and dissipation rate profiles derived from CFD predictions, model predictions of the sediment deposition and cross-sectional concentration profiles of horizontal sediment-laden jets are in excellent agreement with data. Unlike CFD calculations of sediment fall out and deposition from a jet flow, the present method does not require any *a priori* adjustment of particle settling velocity.

Keywords Sediment-laden jets · Turbulence · Particle tracking model · Computational fluid dynamics

S. N. Chan · K. W. Y. Lee
Croucher Laboratory of Environmental Hydraulics, Department of Civil Engineering,
The University of Hong Kong, Hong Kong, China

J. H. W. Lee (✉)
Department of Civil and Environmental Engineering, Hong Kong University of Science and Technology,
Hong Kong, China
e-mail: jhwlee@ust.hk

1 Introduction

Particle-laden jets are commonly found in natural and engineered environments. Volcanic eruption and "black smokers" released from hydrothermal vents in a deep ocean are examples of particle-laden jets in the natural environment. On the other hand, domestic or municipal wastewater is often discharged into coastal waters in the form of multiple jets to maximize the initial dilution. Partially-treated wastewater discharge from marine outfall diffusers often contains organic solids that may settle close to the source, giving rise to the formation of sludge banks and affecting benthic ecology. Modelling the transport and fate of the particulate matters is essential for the quantification and minimization of environmental impact and risks of these harmful particulate discharges.

A number of studies have been carried out for the modelling of deposition of particles from particle-laden jets. Studies with downward vertical particle-laden jets have been carried out to investigate the influence of turbulence on particle dispersion [10,24,26]. In connection with geophysical problems such as volcanic eruptions, studies on the deposition of an upward jet or plume have also been conducted [2,7,20,28]. Limited studies of horizontal sediment-laden jets were also conducted in a very small set-up without adequate theoretical interpretation [1]. However, there is currently no generally accepted theory for predicting the mixing and deposition of horizontal particle-laden water jets and scant data is available to verify theoretical models.

Bleninger et al. [1] performed extensive experiments on the bottom deposition of horizontal sediment-laden jets. They found that the longitudinal sediment deposition is log-normal and the transverse deposition is Gaussian distributed. An analytical deterministic particle tracking model is developed to predict the two-dimensional bottom deposition; the particle trajectory is calculated by assuming constant particle settling velocity in the jet flow, without considering the effect of turbulence. The prediction is found to underestimate the horizontal spread of the particle bottom deposition and the starting point of sedimentation. Lane-Serff and Moran [12] developed a Lagrangian jet model with sediment fall-out in the near source by considering the balance of particle settling velocity and the jet entrainment velocity. Based on the idea of Lane-Serff and Moran [12], Lee et al. [17] developed a two-layer particle jet model based on the Lagrangian jet model JETLAG [14]; the model assumes different concentrations in the upper and lower half of the jet. While the model predicts the correct trends, in order to obtain satisfactory comparison with the laboratory measurements of sediment deposition pattern, the sediment settling velocity has to be reduced by about 30 % by calibration.

The major limitation of previous theoretical models is the lack of understanding on the interaction between turbulence and settling particles. In stagnant water, a sediment particle falls with its terminal settling velocity as a result of the balance of downward gravitational and upward drag forces. Turbulence not only disperses the sediment particles, but also modulates the settling velocity. In turbulent flows, the fluid eddy motion creates additional acceleration (forces) to the particle motion, thus modulating the particle velocity.

Ho [9] measured the settling velocities of spheres in a homogeneous vertically oscillating field of fluid. The apparent settling velocity can be reduced to as much as 40 % of the terminal settling velocity, when the fluid acceleration is about $10g$, where g = gravitational acceleration. Particle settling experiments on oscillating grid turbulence [19,22] showed that the apparent settling velocity is significantly modulated by turbulence; when the ratio of turbulence intensity to terminal settling velocity is less than 3–4, a reduction of settling velocity up to 30 % is observed. Recent studies [6,31] have also shown a maximum settling velocity reduction of 25 % under grid-turbulence. Nevertheless, the effect of jet turbulence on the settling of sediment particles has hitherto not been addressed.

The objective of the present research is to develop a general model to predict the particulate transport and the resultant deposition on the ocean floor in the near and intermediate field of a particle-laden jet discharge. In this paper, the sediment transport and deposition of horizontal particle-laden momentum jets in stagnant water are studied. A stochastic particle tracking model is developed to realistically simulate the sediment concentration and deposition. The model is validated with extensive laboratory experiments. A three-dimensional computational fluid dynamics (CFD) model is also developed for comparison purposes.

2 Problem definition

Figure 1a shows a conceptual model of the structure of a horizontal sediment-laden momentum jet with dilute concentration. The jet with a diameter D and initial velocity u_0 mixes

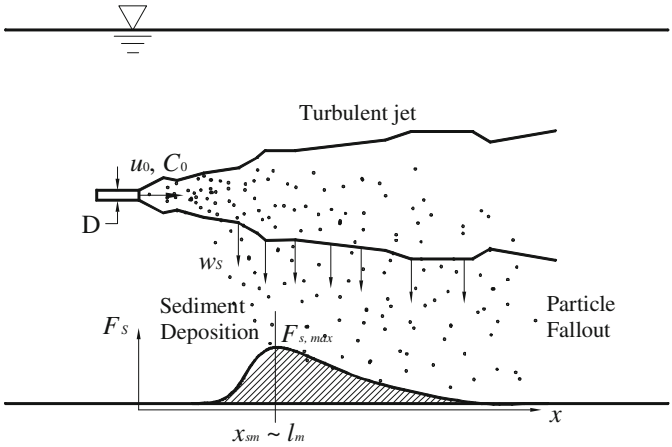

(a) Schematic representation

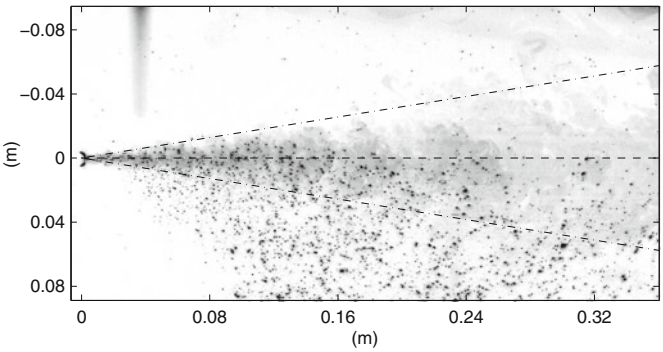

(b) Experimental image for G180J80 $u_0 = 0.88$m/s, $D = 6$mm, $d_{50} = 180\mu$m, $w_s = 1.9$cm/s. The dashed line is centerline of jet; the dash-dotted line is the top-hat boundary defined by $b_T = 0.16x$

Fig. 1 Experiment of horizontal sediment-laden momentum jets. u_0 = jet initial velocity, C_0 = initial sediment concentration, D = jet diameter

with ambient fluid by shear induced turbulent entrainment. Sediment particles with source concentration C_0 and stillwater settling velocity w_s are transported in the horizontal direction and dispersed by turbulent mixing. As the flow velocity and turbulence intensity reduce, particles fall to the bottom under gravity, forming a deposition profile with a peak close to the jet nozzle and an elongated tail. Figure 1b shows a reversed-gray-scale high-speed image taken for a sediment-laden horizontal jet experiment. The fluid flow is coloured by fluorescence dye while the sediments are shown as black spots. The turbulent nature of the jet and the gradual sediment fall-out can be clearly visualized.

The behaviour of a dilute sediment-laden jet is characterized by u_0, D, C_0 and w_s. The jet mixing characteristics can be shown to depend on the integral jet volume flux $Q_0 = u_0 \pi D^2/4$, momentum flux $M_0 = u_0^2 \pi D^2/4$ and the characteristic sediment fall velocity w_s. The sediment deposition rate per unit distance along the jet direction is F_s (g/m/s) with peak value at the distance x_{sm} (Fig. 1a). A momentum-settling length scale $l_m = M_0^{1/2}/w_s$ can be defined to analyze the deposition behaviour of sediment jet [5,12,17]. The importance of jet momentum-induced velocity relative to settling velocity is measured by l_m, which is a measure of the distance from the source to the location where sediment starts to fall out from the jet. Detailed experiments on the structure of horizontal sediment-laden jets have recently been reported [17].

For the experiments in the present study, the sediment concentration is less than 7.7 g/L, corresponding to a volume fraction of less than 0.29 %. Cuthbertson et al. [5] showed experimentally that for sediment volumetric fraction of $\sim$ 0.1 %, the jet trajectory is unaffected by the presence of the sediment. Thus the dilute particle concentration is considered to have little influence on the fluid jet flow.

The details of the formulation of the stochastic particle tracking model is presented with a focus on the particle velocity autocorrelation modeling of settling particles in turbulence. To obtain some insight on the degree of turbulent modulation, the particle tracking model is first applied to predict the apparent settling velocity of particles in a homogeneous turbulent field with zero mean flow. The predicted reduction in settling velocity is consistent with the required reduction in CFD modelling of sediment-laden jets. Finally, a stochastic particle tracking model is developed to predict the deposition from horizontal sediment-laden jets, based on the analytical mean jet flow solution and semi-empirical turbulence quantity profiles derived from CFD modelling. Model predictions are validated by the measured data of sediment deposition and concentration.

3 Lagrangian particle tracking model

3.1 Theory

A three-dimensional discrete particle tracking model with random walk approach is developed based on the work of Nielsen [21]. The particle velocity $\mathbf{u_p}$ is assumed to consist of three parts: (i) the mean flow velocity $\overline{\mathbf{u}}$, (ii) the turbulent fluctuation $\mathbf{u'}$ and (iii) the settling velocity $\mathbf{w_s}$

$$\begin{aligned} \mathbf{u_p} &= \overline{\mathbf{u}} + \mathbf{u'} + \mathbf{w_s} \\ &= \begin{bmatrix} u_p \\ v_p \\ w_p \end{bmatrix} = \begin{bmatrix} \overline{u} \\ \overline{v} \\ \overline{w} \end{bmatrix} + \begin{bmatrix} u' \\ v' \\ w' \end{bmatrix} + \begin{bmatrix} 0 \\ 0 \\ -w_s \end{bmatrix} \end{aligned} \tag{1}$$

With this assumption, the solid particles follow the fluid velocity completely except in the vertical direction. A more comprehensive particle tracking model that solves the full equation of particle motion (including inertia and drag terms) has also been developed. The predicted sediment deposition and concentration profiles for sand and glass particles show little difference with the present simplified model (see later discussion).

The key to modelling settling particles in turbulence lies in the modelling of the turbulent fluctuation $\mathbf{u}'$. According to Taylor's classical analysis on turbulent diffusion [29], the autocorrelation function R of the Lagrangian velocity of a neutrally buoyant particle can be described by an exponential function,

$$R(\Delta t) = \exp\left(-\frac{\Delta t}{T_L}\right) \tag{2}$$

where Δt is the time step size and T_L is the Lagrangian integral time scale for turbulence. To study the dispersion of dust particles suspended in the atmosphere, Csanady [4] extends the autocorrelation function to account for the settling of particles heavier than air and introduced the "cross-trajectory" effect. Csanady's autocorrelation function for particle falling in atmosphere is

$$R(\Delta t) = \exp\left(-\frac{\Delta t}{T_L}\sqrt{1+\frac{w_s^2 T_L^2}{L_z^2}}\right) \tag{3}$$

where w_s is the settling velocity; L_z is the turbulence length scale in the z direction. When the particle is neutrally buoyant ($w_s = 0$), the autocorrelation reverts to that of Taylor's. When $w_s > 0$, the correlation is smaller than Taylor's due to the positive term of $\sqrt{1+\frac{w_s^2 T_L^2}{L_z^2}}$. As explained by Csanady [4], owing to the finite mean settling velocity, the heavier particle continuously changes its fluid-particle neighbourhood and is less correlated than the fluid counterpart when they start from the same location. The reduced correlation means a reduction in dispersion of falling particles. However, this does not explain the reduced settling velocity by turbulence.

Inspired by the experimental observation and analytical derivation of particles trapping in circular vortex flows, Nielsen [21] postulated the "loitering" effect for which particles are trapped in turbulent eddies and delayed from settling. Nielsen has derived an Eulerian equivalent to the autocorrelation function with the loitering assumption that "slow velocity corresponds to small change in velocity", resulting in the following expression for the particle autocorrelation function (see Appendix 1 for the detailed derivation)

$$R_i = \exp\left(-\frac{\Delta t}{T_E}\sqrt{1+A_E\left[\left(\frac{u_i'}{\sigma}\right)^2+\left(\frac{v_i'}{\sigma}\right)^2+\left(\frac{w_i'}{\sigma}\right)^2\right]}\right) \tag{4}$$

In the expression, σ is the root-mean-square (RMS) velocity fluctuation. The subscript i denotes the values in the current time step and Δt is the time-step size. L_E and T_E are the Eulerian spatial and time scale of the turbulence respectively, and $A_E = \frac{\sigma T_E}{L_E}$. If the standard $k-\epsilon$ turbulence closure model [13] is used, L_E and T_E can be estimated as follows:

$$L_E = C_\mu^{3/4}\frac{k^{3/2}}{\epsilon} \tag{5}$$

$$T_E = \sqrt{\frac{3}{2}}C_\mu^{3/4}\frac{k}{\epsilon} \tag{6}$$

$$A_E = \frac{\sigma T_E}{L_E} = 1 \tag{7}$$

where k is the turbulent kinetic energy; ϵ is the turbulent energy dissipation rate; and $C_\mu = 0.09$. The RMS velocity fluctuation is related to the turbulent kinetic energy by

$$\sigma = \sqrt{\frac{2}{3}k}. \tag{8}$$

It is of interest to note that the autocorrelation function Eq. 4 depends on the instantaneous turbulent velocity (u_i', v_i', w_i') and can be viewed as a local adaptation of Taylor's expression. It can be shown that this form of autocorrelation can generate the loitering effect [21] as R_i decreases with increasing instantaneous turbulent velocity. In Appendix 2, using particle imaging velocimetry (PIV) measurements of the jet velocity field, we demonstrate that the jet turbulence can generate the loitering effect.

For a particle with a settling velocity w_s, the autocorrelation function becomes (Appendix 1)

$$R_i = \exp\left(-\frac{\Delta t}{T_E}\sqrt{1 + A_E\left[\left(\frac{u_i'}{\sigma}\right)^2 + \left(\frac{v_i'}{\sigma}\right)^2 + \left(\frac{w_i' - w_s}{\sigma}\right)^2\right]}\right). \tag{9}$$

Interestingly this equation has a similar form as Csanady's autocorrelation function for heavy particles (cf Eq. 3). Equation 9 appears to be applicable to modelling both loitering effect as suggested by Nielsen and the cross-trajectory effect as suggested by Csanady.

Equation 9 can be viewed as a heuristic local correlation that mimics the vortex trapping of sediment particles demonstrated by Nielsen [21]. From Eq. 9, there is an asymmetry between updrafts ($w' > 0$) and downdrafts ($w' < 0$). On an updraft w' and w_s tend to cancel, so the argument of the exponential is closer to 0 and correlation is greater (the exponential function is closer to 1). A particle would tend to retain any upward motion for longer, whereas for a downdraft the motion becomes decorrelated more quickly. Thus on average particles stay in the upward moving flow longer than in the downward moving flow, resulting in the reduction of settling velocity. Extensive numerical experiments have confirmed the characteristic feature of Eq. 9.

With the autocorrelation function, the turbulent fluctuation can be generated by

$$\mathbf{u'_{i+1}} = R_i\mathbf{u'_i} + \chi\sqrt{(1 - R_i^2)}\sigma \tag{10}$$

where the subscript i denotes the current time step and $i + 1$ denotes the next step. χ denotes randomly generated numbers (in x, y, z-directions) following a Gaussian distribution with zero mean and unit variance. With the instantaneous particle velocity determined, the particle position can be found by numerically integrating the velocity with respect to time. The particle position is integrated using a predictor-corrector scheme.

$$\mathbf{x_{i+1}} = \mathbf{x_i} + \frac{1}{2}(\mathbf{u_{i+1}} + \mathbf{u_i})\Delta t. \tag{11}$$

Time step of $\Delta t = 0.001$s is used in the model predictions of sediment settling in homogeneous turbulence and horizontal sediment-laden jets, which is much less than the characteristic time scale of turbulence T_E (in the order of 0.05–0.5 s).

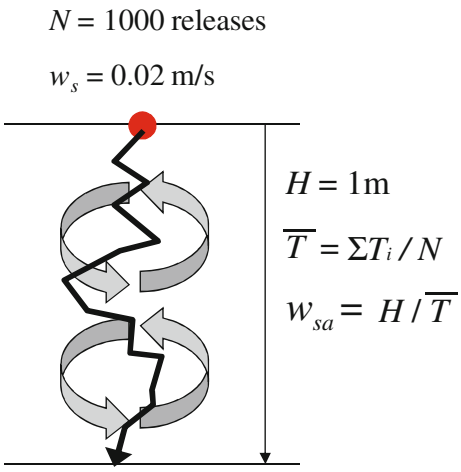

Fig. 2 Schematic representation of a hypothetical experiment of dropping sediment particles in homegeneous turbulence

3.2 Particle settling in homogeneous turbulence

Numerical experiments are carried out to investigate the effect of homogeneous turbulence on the settling velocity. In each hypothetical experiment, $N = 1,000$ particles of stillwater settling velocity 0.02 m/s are allowed to settle for a distance of $H = 1$ m in a field of homogeneous turbulence and zero mean flow (Fig. 2). The turbulence properties are specified with the RMS turbulent velocity fluctuation σ and the turbulence length scale L_E. Various ratio of σ/w_s are specified. L_E is taken as 0.05 m, similar to the grid size used in the grid turbulence experiments of Murray [19]. T_E is computed from Eq. 7 with different A_E specified. The time for falling for 1m for each particle T_i is recorded and the apparent settling velocity w_{sa} is calculated from the mean settling time

$$w_{sa} = H \Big/ \left(\frac{1}{N} \sum_{i=1}^{N} T_i \right). \tag{12}$$

Figure 3 shows the cumulative probability distribution of the apparent settling velocity of four numerical experiments under different ratio of σ to w_s with $A_E = 1$. With increasing turbulence level, the mean apparent settling velocity decreases but the variance in apparent settling velocity increases. This implies that turbulence results in both dispersion of particle and a reduction in the mean settling rate.

Figure 4 shows the settling velocity for different σ to w_s ratios for $A_E = 1$ and 10. The apparent settling velocity reduces as σ/w_s increases. The more intense the turbulence the greater is the delaying effect in settling. The settling velocity reduces by about 20 % for $A_E = 1$ and 30 % for $A_E = 10$ at the highest σ/w_s ratio shown. To provide a functional estimate of the apparent settling velocity, the numerical results for $A_E = 10$ are fitted by a curve in the form of

$$\frac{w_{sa}}{w_s} = (1 + A) - \frac{A}{B + (1 + B)\exp(-C\sigma/w_s)} \tag{13}$$

where $A = 0.265$, $B = 0.459$ and $C = 1.285$ are empirical constants. Equation 13 can also be used to provide approximate estimates of the local reduction of settling velocity as a

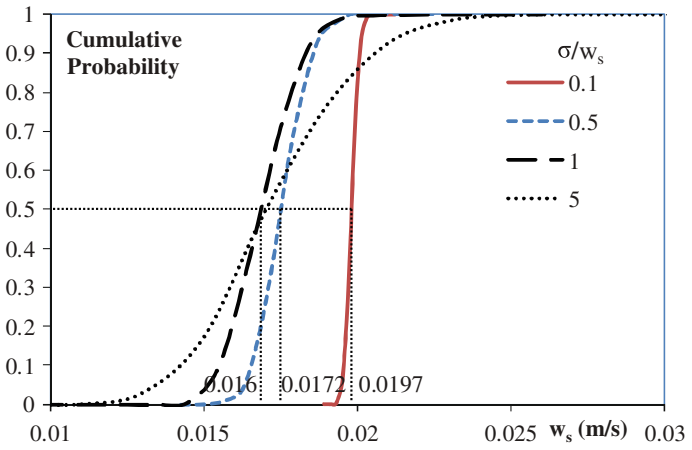

Fig. 3 Cumulative probability distribution of model predicted sediment settling velocities under different σ/w_s with $A_E = 1$ and $L_E = 0.05$ m

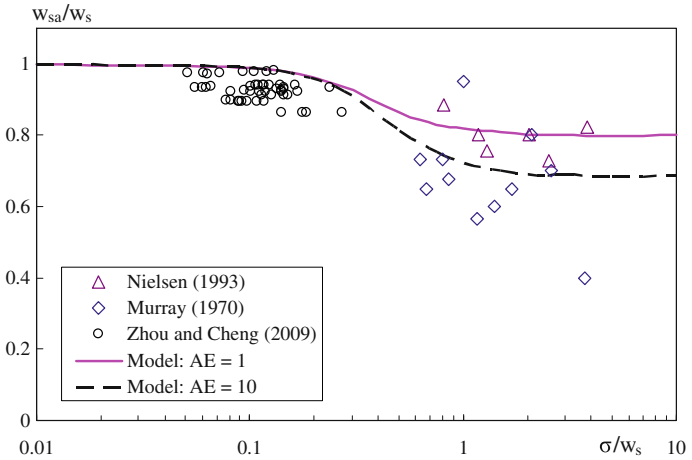

Fig. 4 Comparison of predicted apparent settling velocity ($A_E = 1$ and 10) with the experimental data of particle settling in grid turbulence of Murray [19], Nielsen [22] and Zhou and Cheng [31]

function of the computed RMS fluctuation in a two-equation turbulence model (such as $k-\epsilon$ which assumes isotropic turbulence; see later discussion).

Murray [19] and Nielsen [22] report experiments of particle settling under grid-generated turbulence. Particles with nominal diameter 2 mm [19] and 6.1 mm [22] are used with various particle density to obtain different settling velocity in water. In their experiments, the particle velocity is evaluated by identifying the particle position in subsequent images taken with high-speed camera. The RMS fluid turbulent velocity fluctuation is estimated as the RMS particle velocity fluctuation of neutrally buoyant particles in Murray's experiments [19], and taken as the grid velocity amplitude in Nielsen's experiments [22]. Recently, Zhou and Cheng [31] carried out PIV measurement on sediment settling in grid turbulence. Their σ/w_s ratio is modest, ranging from 0.05 to 0.4 and the result shows a mean reduction of about 10% of the stillwater settling velocity. Despite considerable scatter in the data of [19,22,31] the

model predictions are in broad agreement with the experiments (Fig. 4). Sensitivity tests have shown that even when a larger time-step up to 0.005 s is used, the predicted apparent settling velocity in homogeneous turbulence has less than 1 % difference from that using a time-step of 0.001 s.

4 Modelling of horizontal sediment-laden jets

4.1 Laboratory experiments

Experiments of horizontal momentum sediment-laden jet in stagnant ambient (Fig. 1) are carried out in a 1 m × 1 m × 0.5 m height water tank with nozzle diameter $D = 6$ mm. An overhead tank is used for steady flow supply with jet flow rate controlled by a calibrated rotameter. The sediment particles are fed to the jet flow at a constant rate using an hourglass. Details of the experiments are described in Lee [16] and Li [18]. In the following we give only the essential details needed for the experimental validation of the numerical model predictions.

Natural quartz sand [18] and synthetic glass particles [16] are used in the experiments. Natural sand particles have a density ρ_s of 2.65 g/cm^3, sieved into two different size ranges: 150–212 μm as "Coarse Sand" and 62–150 μm as "Fine Sand". Synthetic spherical glass particles have a density of 2.5 g/cm^3 with median diameter 115, 180 and 215 μm; they are more uniform in size, density and optical properties than natural sand.

The particles used in the present study have settling velocity around 1–2 cm/s. For glass particles, the settling velocity is estimated using the median diameter d_{50} with the drag coefficient for spherical particles.

$$
\begin{aligned}
w_s &= \sqrt{\frac{4}{3}\frac{(s-1)gd_{50}}{C_D}} \\
C_D &= f(Re_p) = \frac{24}{Re_p}\left(1 + 0.15Re_p^{0.687}\right) + \frac{0.42}{1 + 42500Re_p^{-1.16}} \\
Re_p &= \frac{d_{50}w_s}{\nu}
\end{aligned}
\tag{14}
$$

where $s = \rho_s/\rho_w$ is the specific gravity; C_D is the drag coefficient [3]; Re_p is the particle Reynolds number; ν is the kinematic viscosity of water.

For natural sand particles, the settling velocity is obtained from direct measurement using a settling column. The equivalent diameter d_{eq} is inferred from the measured settling velocity with the semi-empirical formula of Soulsby [27]:

$$
\begin{aligned}
w_s &= \frac{\nu}{d_{eq}}\left[(10.36^2 + 1.049D_*^3)^{1/2} - 10.36\right] \\
D_* &= \left[\frac{g(s-1)}{\nu^2}\right]^{1/3} d_{eq}
\end{aligned}
\tag{15}
$$

To measure the sediment deposition rate, a bottom tray is used for the sediment collection. The jet nozzle is located at a distance of 7 cm above the tray for Li's experiments [18] and 15 cm for Lee's experiments [16]. The sediment collected from the bottom tray are oven-dried and weighed for mass. The mass recoveries (collected mass/input mass) of the experiments are over 90 %. Figure 12(a) shows a typical sediment deposition pattern of

Table 1 Summary of horizontal sediment-laden jet experiments for bottom deposition and cross-sectional sediment concentration measurement

Particle type	Particle diameter d_{eq} (μm)	Settling velocity w_s (cm/s)	Jet flow rate Q_j (L/h)	Jet velocity u_0 (m/s)	Jet Reynolds number $Re = \frac{u_0 D}{\nu}$	Sediment concentration C_0 (g/L)	Momentum/ settling length scale l_m/D
Li [18], sediment bottom deposition measurement, $\rho_s = 2.65\,\text{g/cm}^3$							
Coarse sand (CJ)	166	1.98	50, 54, 58, 62, 66	0.49–0.65	2,940 −3,900	3.39–4.49	22.2–29.2
Fine sand (FJ)	133	1.41	30, 34, 38, 42, 46, 50, 54, 58	0.30–0.57	1,800 −3,420	3.93–7.73	18.5–35.7
Lee [16], sediment bottom deposition and concentration measurement, $\rho_s = 2.5\,\text{g/cm}^3$							
Spherical glass 215 μm (G215J)	215	2.64	60, 70, 80, 90	0.57–0.86	3,970 −5,650	3.39–4.49	18.9–28.3
Spherical glass 180 μm (G180J)	180	1.83	50, 60, 70, 80	0.48–0.76	2,980 −4,660	2.32–3.71	20.6–32.9
Spherical glass 115 μm (G115J)	115	1.03	40, 50, 60, 70	0.38–0.67	2,630 −4,430	1.03–1.83	32.9–57.6

Jet diameter $D = 6\,\text{mm}$, l_m = momentum-settling length scale = $M_0^{1/2}/w_s$, ν = water viscosity = $10^{-6}\text{m}^2/\text{s}$

one of the experiments. An innovative particle imaging technique is developed for particle concentration measurement across the jet sections using spherical glass particles in dilute concentration [16,17]. It is extensively compared with suction sampling measurement and checked by mass balance with the bottom deposition rate.

Table 1 summarises the experiments used for comparison with the numerical predictions. The experiments are labeled in the way of "XJQ_j". 'X' denotes the type of sediment: 'C' represents the coarse natural sand; 'F' for fine natural sand; 'G215', 'G180' and 'G115' represent the spherical glass particles in their d_{50} in μm respectively. 'Q_j' is the jet flow rate in L/h. For example CJ66 is an experiment using coarse natural sand with jet flow rate 66 L/h ($u_0 = 0.68$ m/s). All experiments are essentially turbulent as the jet Reynolds number is greater than 1,800.

4.2 3D computation fluid dynamics (CFD) model

4.2.1 Governing equations

A three-dimensional CFD model is employed to study the concentration and deposition pattern of horizontal sediment jets, and provides the turbulence quantities for the particle tracking model developed in this study (Sect. 4.3). The 3D Reynolds-averaged Navier–Stokes equations are solved for incompressible steady state:

$$\frac{\partial U_i}{\partial x_i} = 0 \tag{16}$$

$$U_j \frac{\partial U_i}{\partial x_j} = -\frac{1}{\rho_f}\frac{\partial p}{\partial x_i} + \frac{\partial \tau_{ij}}{\partial x_j} \tag{17}$$

where U_i is the fluid velocity in x, y and z directions; ρ_f is the density of fluid; p is the dynamic pressure; τ_{ij} is the Reynolds stresses estimated as with the gradient transport analogy:

$$\tau_{ij} = \nu_t \left(\frac{\partial U_j}{\partial x_i} + \frac{\partial U_i}{\partial x_j} \right) - \frac{2}{3} k \delta_{ij} \tag{18}$$

where ν_t is the eddy viscosity estimated by the realizable $k-\epsilon$ turbulence closure model [25] solving for the turbulent kinetic energy k and dissipation rate ϵ. The model differs from the standard $k-\epsilon$ model in two important ways: (i) The eddy viscosity coefficient C_μ is not a constant, but determined as a function of k, ϵ, and the local strain rate ; and (ii) a new and more physically realistic transport equation for the dissipation rate is used. The realizable $k-\epsilon$ model guarantees positivity of the normal Reynolds stresses, and gives accurate prediction of the spreading rate for both planar and round jets [25]. For the present jet flow cases, the predicted spreading rate of jet half width is 0.12, comparable with the experimentally measured value of 0.114 [8,15] and better than the value of 0.13–0.14 obtained using the standard $k-\epsilon$ model.

The equation for sediment transport, assuming very dilute concentration, is

$$(U_j - w_{sa,j})\frac{\partial C}{\partial x_j} = \frac{\partial C}{\partial x_j}\left(\frac{\nu_t}{Sc_t}\frac{\partial C}{\partial x_j} \right), \quad w_{sa,j} = \begin{bmatrix} 0 \\ 0 \\ -w_{sa} \end{bmatrix} \tag{19}$$

where C is the sediment concentration and Sc_t is the turbulent Schmidt number taken as 0.85. The term $w_{sa}\frac{\partial C}{\partial z}$ is added for the settling flux of sediment, where w_{sa} is the apparent settling velocity, estimated as a function of the RMS turbulence fluctuation (turbulent kinetic energy) using Eq. 13.

4.2.2 Boundary and initial conditions

Inflow velocity and sediment concentration are prescribed at the jet nozzle. The turbulent kinetic energy k is estimated from well-established relations for fully developed smooth pipe flow, $k = \frac{3}{2}(uI)^2$, where u = inflow velocity, I = turbulence intensity related to the Reynolds number via the Blassius equation $I = 0.16Re^{-1/8}$. The value of ϵ at the inlet is then given by $\epsilon = C_\mu^{3/4}\frac{k^{3/2}}{l}$; l is the length scale of energy containing eddies and adopted as $l = 0.07D$ similar to the mixing length. For the bottom and wall adjacent to the jet nozzle, a no slip wall boundary is used. For other boundaries, a zero pressure condition is used, and k and ϵ are specified as 1 % of the values of the jet inlet. By virtue of symmetry about the vertical jet centerline plane (the x–z plane), only half of the tank is modelled. For the sediment transport, a zero flux boundary condition is applied on all boundaries except at the bottom where sediment flux $w_{sa}C$ is prescribed.

Zero velocity, pressure and sediment concentration are prescribed as initial values for iteration. The initial k and ϵ in the whole domain are specified as 0.01 times the values of the inlet. Sensitivity tests show that the prescribed initial values of k and ϵ do not have a significant effect on the final steady flow, since the turbulence in the tank will evolve as the flow develops from the inlet.

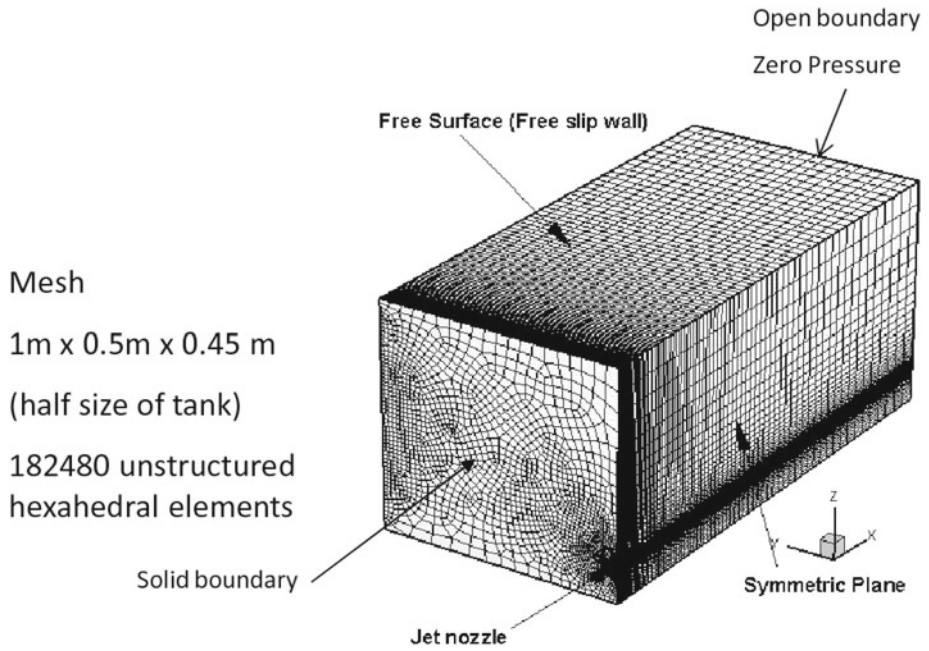

Fig. 5 Computation mesh for horizontal sediment-laden jets

4.2.3 Grid configuration and computational details

A three-dimensional unstructured mesh with 182,420 non-uniform hexahedral elements is used to discretise the half-experimental tank and jet nozzle with diameter of 6 mm (Fig. 5). The smallest mesh size in the direction of the jet is 6 mm, about 1/10 of the length of the zone of flow establishment. The smallest transverse mesh size at the jet nozzle is of size 0.6 mm, 1/10 the diameter of the jet nozzle. The jet tube is not separately modelled but located on the same plane with the wall of the jet inlet.

The governing equations are solved numerically using the finite volume method as embodied in the FLUENT software. Velocities and other variables are defined at the cell center. Cell face dependent variables are interpolated from the cell center values using a second order upwind scheme. The SIMPLEC algorithm is employed for velocity–pressure correction with under-relaxation factor of 0.3 for pressure, 0.7 for momentum, 0.8 for k and ϵ, and 1.0 for turbulent viscosity and sediment concentration. Convergence is declared when the normalized residual is less than 10^{-6} for sediment concentration and 10^{-3} for all other variables. Typically about 5,000 iterations are required for convergence. Similar numerical settings can be found in Kuang and Lee [11]. Grid convergence tests have shown that the jet centerline velocity and maximum sediment deposition differs by less than 3 % even when the grid size is doubled.

4.2.4 CFD results

CFD computations have been carried out for all experiments in Table 1 (jet diameter = 6 mm) with different jet initial velocity u_0, sediment concentration C_0 and sediment settling velocity w_s. Figures 6 and 7 shows an example of the CFD predicted mean velocity and

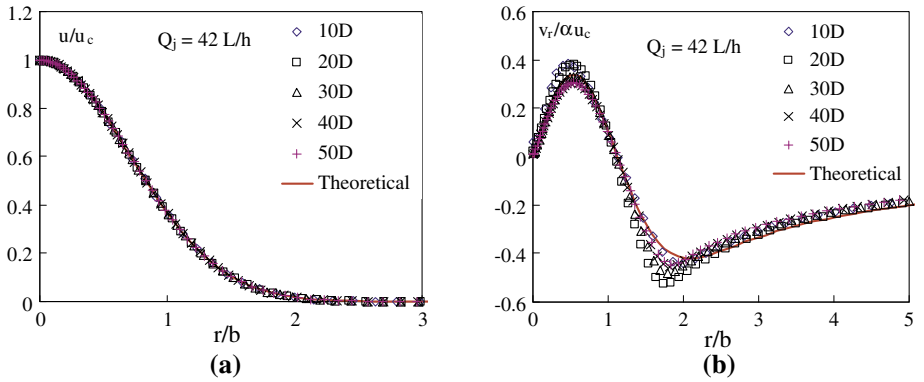

Fig. 6 Theoretical (analytical solution) and CFD predicted jet mean velocity profiles. **a** Longitudinal velocity, Eq. 21, **b** transverse velocity, Eq. 22

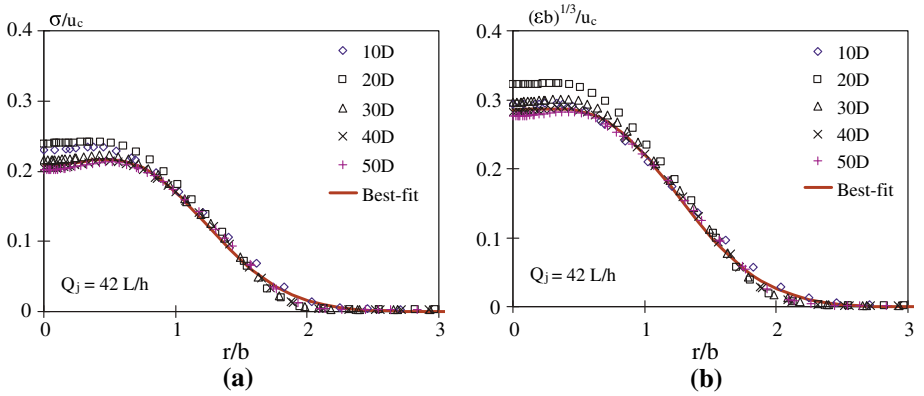

Fig. 7 Turbulent velocity fluctuation and dissipation rate dissipation, predicted by CFD model and fitted with empirical equations. **a** RMS turbulent velocity fluctuation, Eq. 23, **b** Turbulent energy dissipation rate, Eq. 24

turbulence quantities for jet initial velocity of 0.41 m/s (jet flow rate = 42 L/h). The CFD predicted transverse distribution of axial velocity profile at different cross-sections are self-similar and can be normalized against the centerline velocity u_c and a characteristic jet width b (defined by $u(b)/u_c = \exp(-1)$) (Fig. 6a). The radial jet velocity also compares well with the classical analytical solution of a momentum jet (Fig. 6b, see Eq. 22). The predicted RMS turbulent fluctuation σ and turbulent energy dissipation rate ϵ also shows self-similarity upon a suitable normalization (see Sect. 4.3.2). Making reference to this result on grid-generated turbulence, the locally reduced settling velocity w_{sa} in a particle-laden jet can be estimated using the computed σ for predicting bottom deposition profiles (Fig. 8).

4.3 3D Stochastic particle tracking model

4.3.1 Mean velocity field (analytical solution)

The particle tracking model is developed to predict the deposition rate and profiles of the sediment-laden jets experiments using the extensively validated theoretical mean flow veloc-

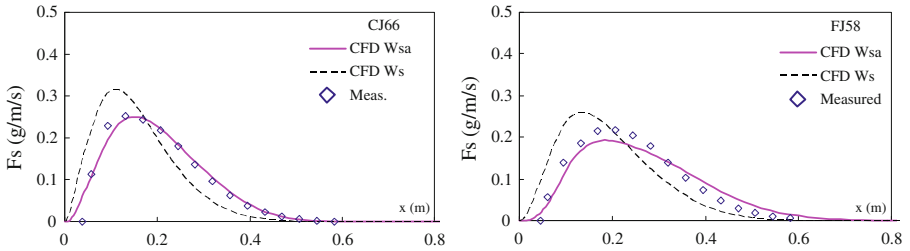

(a) Run CJ66: $d_{eq} = 166\mu m$, $u_0 = 0.65 m/s$, $w_s = 1.97 cm/s$

(b) Run FJ58: $d_{eq} = 133\mu m$, $u_0 = 0.57 m/s$, $w_s = 1.41 cm/s$

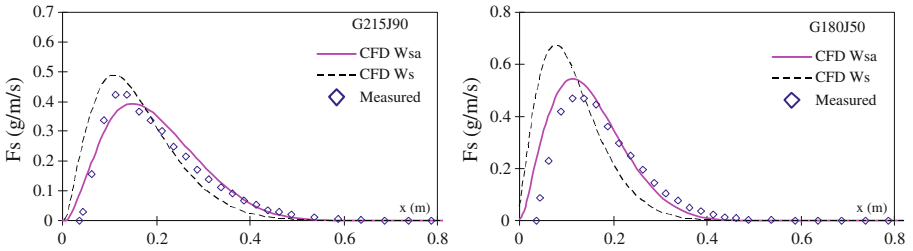

(c) Run G215J90: $d_{50} = 215\mu m$, $u_o = 0.86$ m/s, $w_s = 2.66$ cm/s

(d) Run G180J50: $d_{50} = 180\mu m$, $u_o = 0.49$ m/s, $w_s = 1.96$ cm/s

Fig. 8 Observed and CFD predicted longitudinal particle deposition pattern of four experiments using sand and glass particles. The *solid line* is predicted using the corrected settling velocity w_{sa} using Eq. 13. The *dashed line* is predicted using the terminal settling velocity w_s

ity field of a simple jet and semi-empirical RMS turbulent velocity fluctuation and turbulent dissipation rate profiles derived from CFD modelling. The jet mean longitudinal velocities are given by (e.g. Fischer et al. [8])

$$\frac{u_c(x)}{u_0} = 6.2\left(\frac{x}{D}\right)^{-1} \tag{20}$$

$$\frac{u(x,r)}{u_c(x)} = \exp\left(-\frac{r^2}{b^2}\right) \tag{21}$$

where u_c is the jet centerline velocity, u_0 is the initial velocity, D is the initial jet diameter and $b = \beta x$ is the Gaussian half width and $\beta = 0.114$ is the jet linear spreading rate. The mean transverse velocity of the jet is given by the following expression deduced by applying continuity to the jet cross-section [15]

$$\frac{v_r(r)}{\alpha u_c} = \frac{(1-\exp(-r^2/b^2)) - (\beta/\alpha)(r^2/b^2)\exp(-r^2/b^2)}{r/b} \tag{22}$$

where $v_e = \alpha u_c$ is the entrainment velocity at the edge of the jet, $r = b$, and $\alpha = 0.057$ is the entrainment coefficient. Figure 6 shows the mean velocity profiles of a jet and the comparison with CFD prediction.

4.3.2 Turbulence quantities

Assuming isotropic turbulence, the RMS turbulent fluctuation σ is obtained from the turbulent kinetic energy k according to Eq. 8 using a $k-\epsilon$ turbulence closure model with CFD

simulation of a pure jet (see Sect. 4.2). The CFD predicted σ and ϵ are normalized with the mean jet properties as $\frac{\sigma}{u_c}$ and $\frac{(\epsilon b)^{1/3}}{u_c}$ respectively, and fitted with an equation with the form of

$$\frac{\sigma(r)}{u_c} = C_1\left[\exp\left(-C_2\left(\frac{r}{b}-C_3\right)^2\right)+\exp\left(-C_2\left(\frac{r}{b}+C_3\right)^2\right)\right] \tag{23}$$

and

$$\frac{(\epsilon(r)b)^{1/3}}{u_c} = C_4\left[\exp\left(-C_5\left(\frac{r}{b}-C_6\right)^2\right)+\exp\left(-C_5\left(\frac{r}{b}+C_6\right)^2\right)\right] \tag{24}$$

to provide their spatial functions. The empirical coefficients

$$\begin{bmatrix} C_1 \\ C_2 \\ C_3 \end{bmatrix} = \begin{bmatrix} 0.2006 \\ 1.4147 \\ 0.6647 \end{bmatrix}, \begin{bmatrix} C_4 \\ C_5 \\ C_6 \end{bmatrix} = \begin{bmatrix} 0.2458 \\ 1.2498 \\ 0.6594 \end{bmatrix}$$

are obtained using least-square best-fitting. The turbulence length and time scales L_E and T_E in the autocorrelation function Eq. 9 can then be estimated from Eqs. 5 and 6 at any location using σ (or k) and ϵ. Figure 7 shows the normalized radial distribution of turbulence quantities in a jet. The fitted equations also compare favourably with the computed σ and ϵ profiles of other jet flow cases. The RMS turbulent velocity fluctuation profiles compare very well to the experimental measurement by Papanicolaou and List [23] and Wang and Law [30] with a centerline turbulence intensity of about 0.22, within the range of the previous studies. A slightly higher σ/u_c and ϵ is obtained by the CFD model at $x = 20D$. Inclusion of this effect in the particle tracking model is tested and found to be insignificant for predicting the deposition pattern. Thus a single normalized turbulent quantity profile is used for all longitudinal locations.

4.3.3 Computational procedure

The stochastic particle tracking is performed using Eqs. 1, 9, 10 and 11 with the mean jet flow velocity determined from Eqs. 20–22, and turbulent quantities from Eqs. 23 and 24. $N_p = 50,000$ particles are used for each jet simulation to obtain the deposition profile. Each particle shares an equal fraction of the total sediment mass used in the experiment ($M_i = Q_j C_0 T_{exp}/N_p$). T_{exp} is the total duration of the numerical experiment, which is set as 5 min. The particles are released at the end of the zone of established flow ($x = 6.2D$) according to a Gaussian distribution and tracked until they reach the level of the bottom tray (depends on the experiments). The 1D longitudinal deposition rate (in the unit of g/m/s) profiles are obtained by summing all particles at the y-direction under intervals of $\Delta x = 0.02$ m at the x-direction and divided by the experiment time T_{exp}. The 2D longitudinal deposition rate (in the unit of g/m^2/s) are obtained by summing all particles within grid cell size of $\Delta x = 0.045$ m and $\Delta y = 0.015$ m and divided by the experiment time T_{exp}. Particle tracking calculations have been performed for all experiments in Table 1 using a time-step of 0.001 s and selected results are shown in the next section. Sensitivity tests have shown that even when a larger time-step up to 0.005 s is used, the predicted maximum deposition rates differ by less than 3 %.

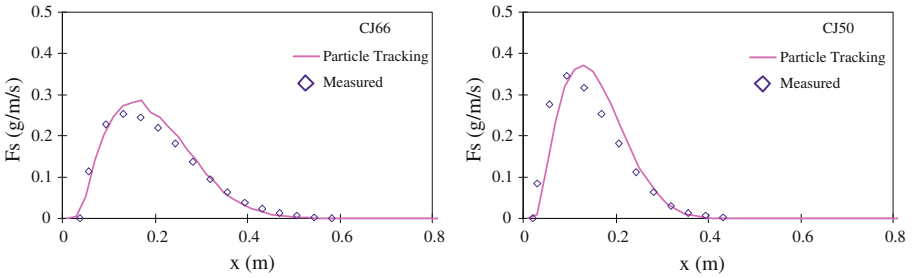

(a) Run CJ66: $d_{eq} = 166\mu m$, $u_0 = 0.65 m/s$, $w_s = 1.97 cm/s$

(b) Run CJ50: $d_{eq} = 166\mu m$, $u_0 = 0.49 m/s$, $w_s = 1.97 cm/s$

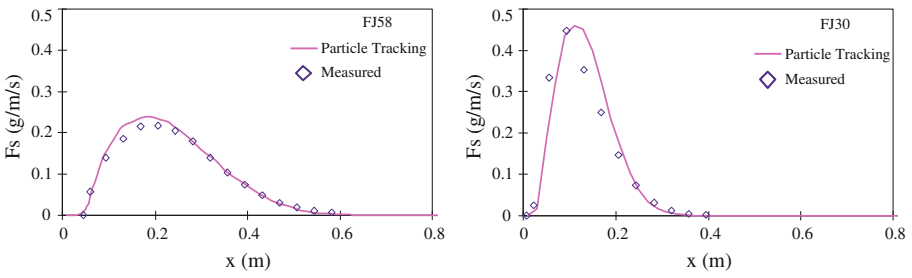

(c) Run FJ58: $d_{eq} = 133\mu m$, $u_0 = 0.57 m/s$, $w_s = 1.41 cm/s$

(d) Run FJ30: $d_{eq} = 133\mu m$, $u_0 = 0.29 m/s$, $w_s = 1.41 cm/s$

Fig. 9 Comparison of measured and particle tracking predicted deposition rate profiles of experiments using natural sand particles

5 Results

5.1 Deposition rate profiles

Figure 8 shows the comparison of the sediment deposition profiles by laboratory measurement and CFD for four representative experiments with sand and glass particles. When the stillwater settling velocity is used in the Eulerian CFD model, the resultant deposition profile is not in good agreement with the experimental measurement. A higher maximum deposition rate is predicted with its position closer to the jet nozzle. This indicates the importance of jet turbulence in reducing the settling velocity. If the settling velocity is corrected with the turbulence level according to Eq. 13, a much closer comparison is obtained. This correction function applies to all the experimental cases using natural sand and glass particles in this study. On the other hand, based on the CFD predicted fields of RMS turbulent fluctuation and dissipation rate, the particle tracking model predicts the deposition pattern very well without the need of any *a priori* correction to the settling velocity to account for turbulence (Fig. 9). The model predicts equally well for spherical glass particles (Fig. 10).

The ratios of RMS turbulent fluctuation to terminal settling velocity σ/w_s in various cross-sections of a jet illustrate the degree of interaction between turbulence and sediment (Fig. 11). Within two Gaussian width b the RMS turbulent fluctuation is very high and nearly 4 times of the settling velocity. Near the centerline of the jet, a reduction close to 30 % of the terminal settling velocity is possible (Fig. 11b). This value is consistent with the reduction

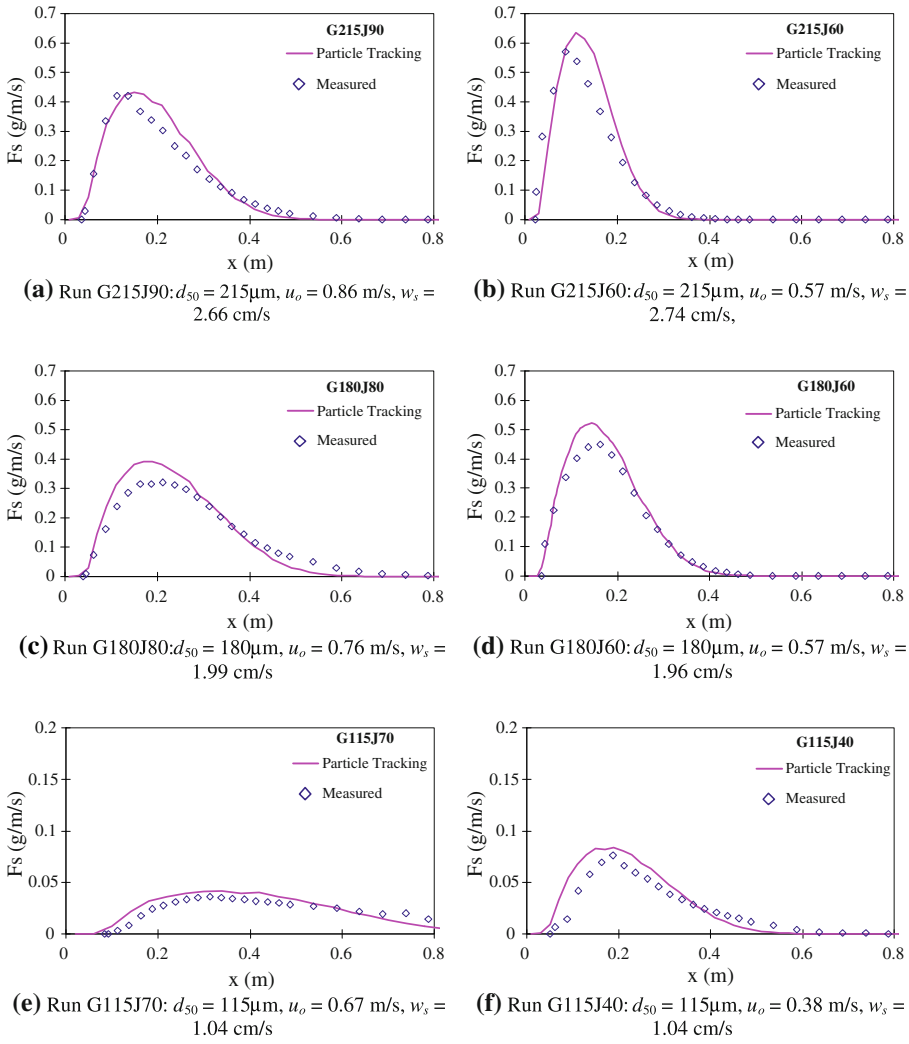

(a) Run G215J90: d_{50} = 215μm, u_o = 0.86 m/s, w_s = 2.66 cm/s

(b) Run G215J60: d_{50} = 215μm, u_o = 0.57 m/s, w_s = 2.74 cm/s,

(c) Run G180J80: d_{50} = 180μm, u_o = 0.76 m/s, w_s = 1.99 cm/s

(d) Run G180J60: d_{50} = 180μm, u_o = 0.57 m/s, w_s = 1.96 cm/s

(e) Run G115J70: d_{50} = 115μm, u_o = 0.67 m/s, w_s = 1.04 cm/s

(f) Run G115J40: d_{50} = 115μm, u_o = 0.38 m/s, w_s = 1.04 cm/s

Fig. 10 Comparison of measured and particle tracking predicted deposition rate profiles of experiments using spherical glass particles

factor used by Lee et al. [17] for its jet integral model which is merely obtained by fitting with experimental data. The reduction decreases as the radial position increases. When $r > 2b$, the terminal settling velocity resumes as the jet turbulence no longer influences the particle settling.

Figure 12 shows the observed and particle-tracking predicted sediment deposition profile of one experiment, CJ58. Meandering of the deposition can be observed which is possibly due to the secondary current induced by jet entrainment of ambient fluid in a finite-sized tank. Nevertheless, the transverse spreading of the particles are well predicted by the particle tracking model.

Comparison of measured and predicted 2D deposition profiles are shown in Figs. 13 and 14. The predicted longitudinal and transverse extent of the deposition compares reasonably

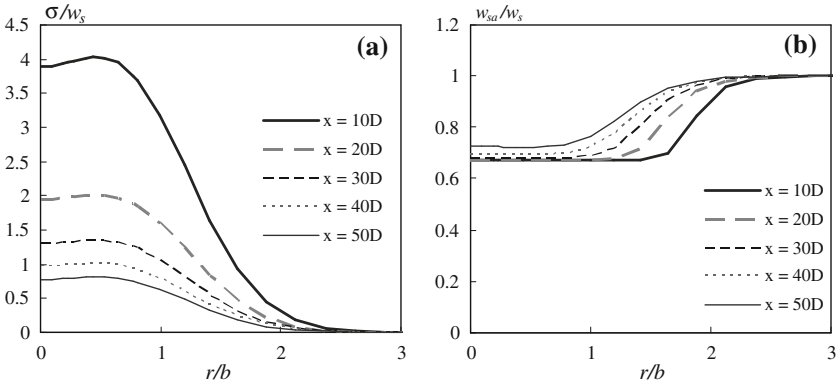

Fig. 11 **a** Ratio of RMS turbulent velocity to settling velocity (σ/w_s), and **b** ratio of apparent settling velocity to terminal settling velocity (w_{sa}/w_s), in different cross-section of a jet. Jet case FJ42: $d_{eq} = 133\,\mu$m, $u_0 = 0.41$ m/s, $w_s = 1.41$ cm/s

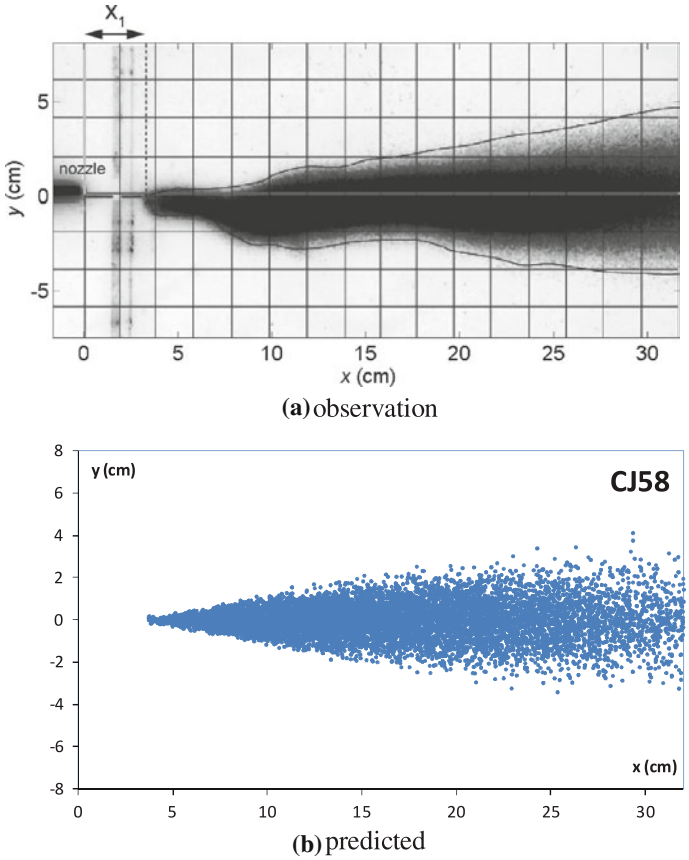

Fig. 12 Observed and predicted (particle tracking) deposition pattern in a horizontal sediment jet experiment (CJ58, $d_{eq} = 166\,\mu$m, $u_0 = 0.57$ m/s, $w_s = 1.97$ cm/s)

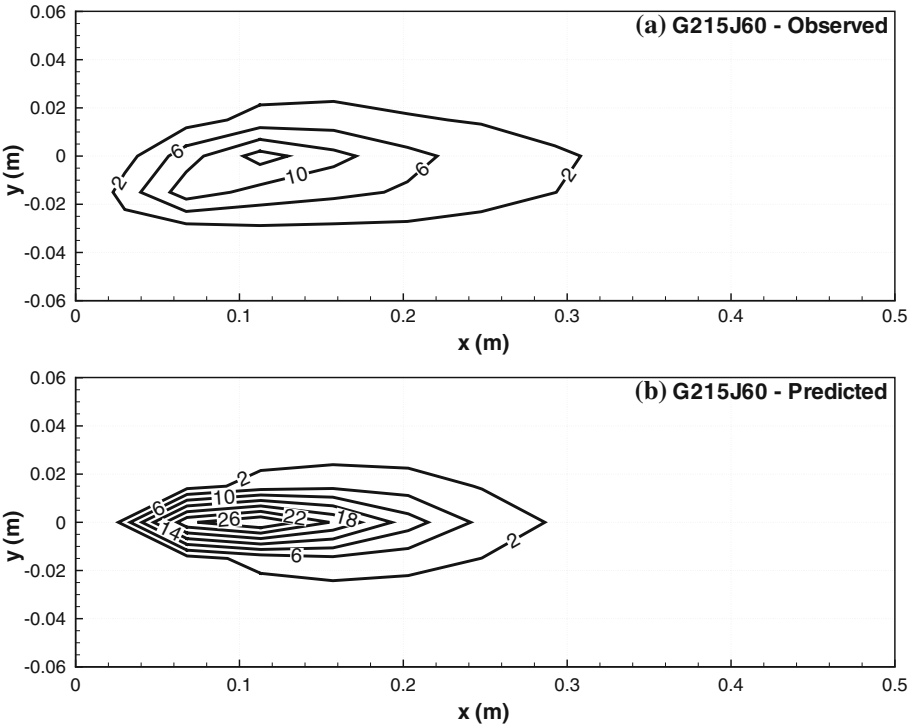

Fig. 13 Observed and predicted deposition profile in a sediment jet experiment (G215J60, $u_0 = 0.58$ m/s, $d_{50} = 215\,\mu$m, $w_s = 2.65$ cm/s). Sediment deposition contour in g/m^2/s. The jet nozzle is located at $x = 0,\ y = 0$

well with the observations. Similar with the sand experiments, the deposition profile is not symmetric in the transverse direction, except for the cases with low jet velocity and high settling velocity. The closer to the jet nozzle, the greater is the asymmetry in the profile. In addition, the predicted transverse spread is smaller than observation, leaving a higher peak at the centerline. Cross-section particle concentration measurement [16,17] (see also Fig. 16) shows that as particles fall out from the turbulent jet, they are not falling vertically as expected, but with an inclined trajectory. The particle trajectories are not stable, but tend to swing across the cross-section periodically. It implies that the external entrainment flow is not stable, probably due to the limited size of the experimental tank and the interaction with the settling particles. This is probably the reason for the asymmetry and the increased spread of the observed deposition profiles. In the particle tracking model, such complex flow phenomenon has not been included.

5.2 Sediment concentration profiles

The predicted cross-sectional sediment concentration profiles are compared with the laboratory data of [16] measured by particle imaging technique. Transformation of particle mass to sediment concentration is required for the discrete particle tracking model. Within a control volume $\Delta V = \Delta x \Delta y \Delta z$, the concentration can be evaluated by the average number of particles inside the control volume. The transverse grid size (Δy and Δz) is defined as one

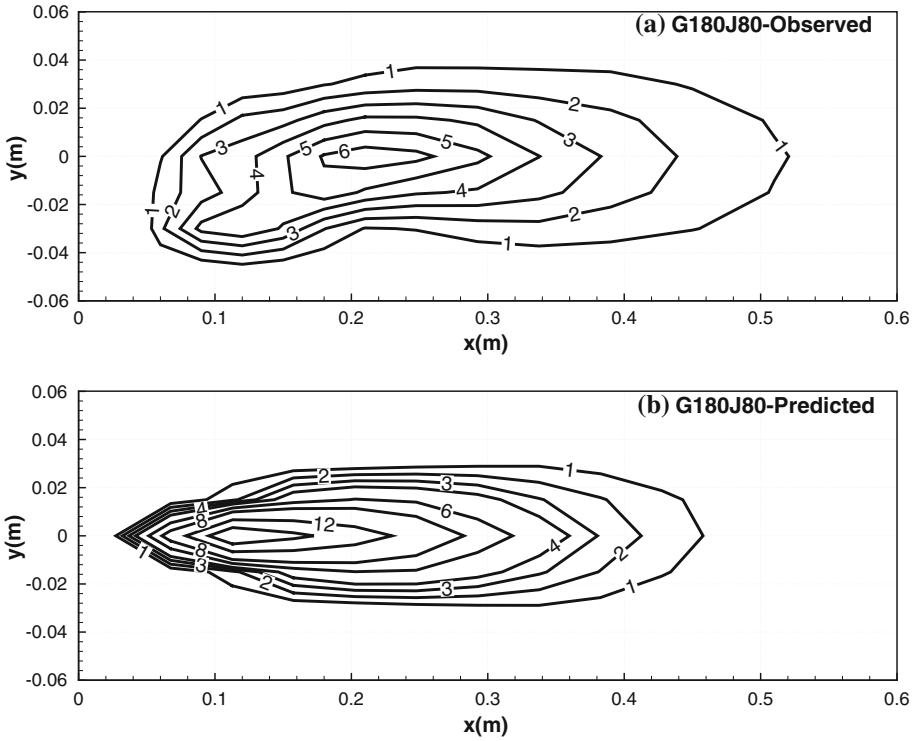

Fig. 14 Observed and predicted deposition profile in a sediment jet experiment (G180J80, $u_0 = 0.78$ m/s, $d_{50} = 180\,\mu$m, $w_s = 1.98$ cm/s). Sediment deposition contour in g/m^2/s. The jet nozzle is located at $x = 0$, $y = 0$

sixth of the top-hat width, similar to the grid size used in particle imaging measurement. The thickness of the grid $\Delta x = 3$ mm.

Figures 15 and 16 show the comparison of measured and particle tracking predicted cross-sectional sediment concentration profiles of two of the experimental cases: G215J60 and G180J80. The sediment concentration profiles in three longitudinal locations, respectively, $x < l_m$, $x \approx l_m$ and $x > l_m$, are shown, where l_m is the momentum-settling length scale [17]. The top-hat profile of the jet, defined as $b_T = 0.161x$, is included as a reference. The predicted cross-sectional concentration contours in general compares well with the experimental measurements. The particle concentration across the sediment momentum jet is in general horseshoe-shaped, except in a region close to the jet nozzle where jet momentum dominates over settling (high jet velocity vs small settling velocity). The vertically parallel contours on the open side at the bottom reflect the particle settling from the lower jet edge. For $x < l_m$, the upper half of sediment jet behaves like a pure jet with axisymmetric concentric contours. The vertical location of maximum particle concentration C_m is approximately at the center of the jet. For $x \approx l_m$, the sediment cloud starts to depart from the water jet; the location of maximum concentration starts to move downwards, but still well within the top-hat jet boundary. The concentration pattern is much elongated in the vertical direction and becomes elliptic. For $x > l_m$, the particle cloud separates significantly from the water jet; the location of maximum particle concentration is moved down to the lower half of the jet or outside

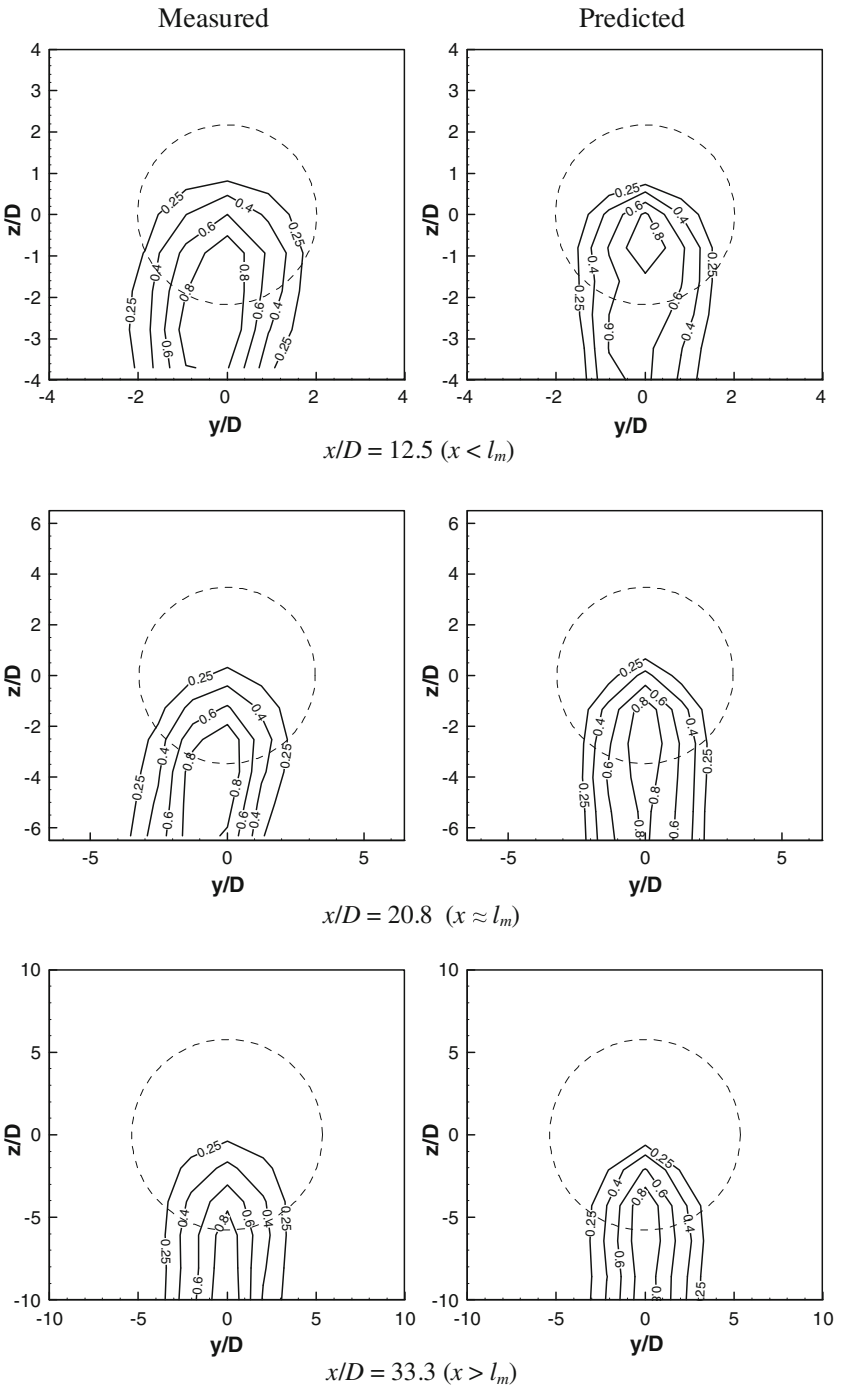

Fig. 15 Measured and particle tracking predicted cross-sectional sediment concentration, case G215J60, $l_m/D = 18.9$. *Dashed circle* represents the top-hat profile of the jet

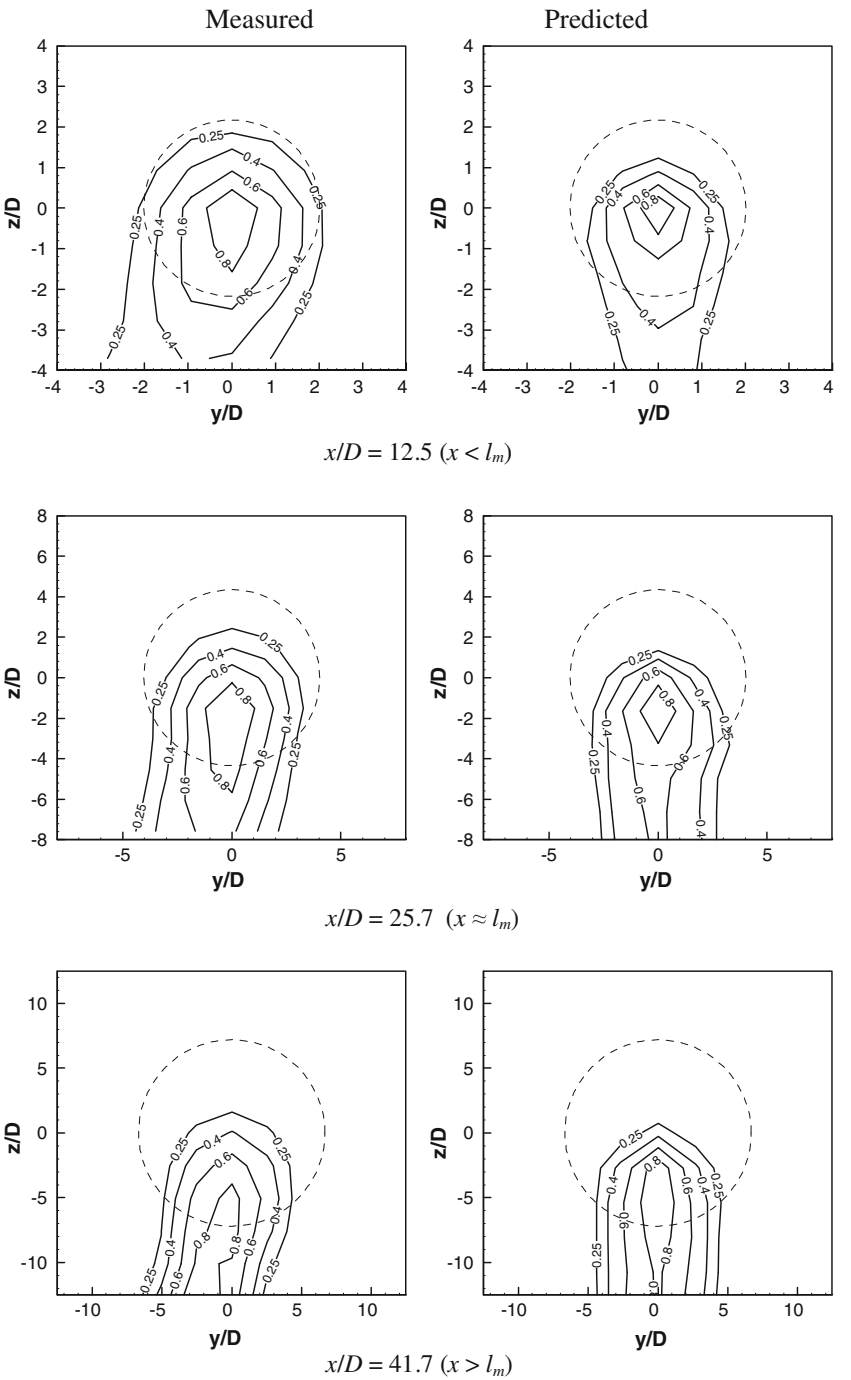

Fig. 16 Measured and particle tracking predicted cross-sectional sediment concentration, case G180J50, $l_m/D = 32.9$. *Dashed circle* represents the top-hat profile of the jet

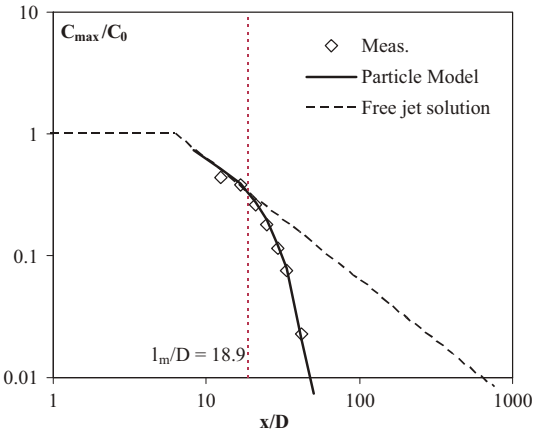

(a) RunG215J60: u_0 =0 .57m/s, w_s =2 .66cm/s, l_m/D =18 .9

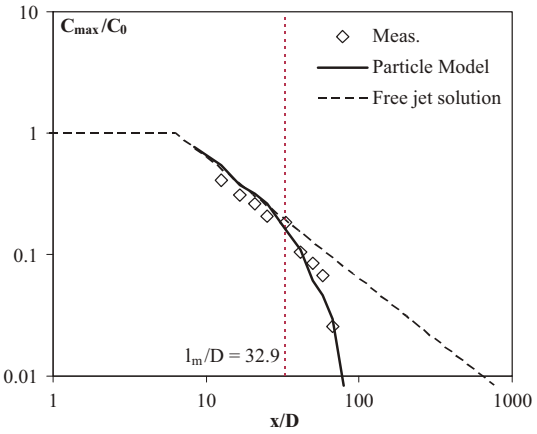

(b) RunG180J80: u_0 =0 .76m/s, w_s =1 .99cm/s, l_m/D =32 .9

Fig. 17 Measured and particle tracking predicted centerline maximum concentration. *Dashed line* is the theoretical tracer concentration variation for a free jet

jet region. In the measurement, the horseshoe trail is often skewed to one side reflecting the asymmetry and complexity of the external entrainment flow.

The comparison of predicted and measured maximum sediment concentration at the centerline plane is shown in Fig. 17 for the same two cases. The measurement and predicted concentrations compares very well. When $x < l_m$, the sediment concentration lies very close to the theoretical centerline concentration profile for a simple jet with neutral buoyant tracers. As $x > l_m$, the centerline maximum concentration departs rapidly from the free jet solution due to the massive fall out of sediment particles.

6 Conclusions

A stochastic particle tracking model is developed to investigate the interaction between turbulence and sediment particles, with a focus on horizontal sediment-laden momentum

jets. Particle velocity fluctuations in the turbulent flow are modelled using a Lagrangian autocorrelation function that accounts for the "loitering" effect which delays particle settling in turbulent eddies. It is found that a significant reduction up to about 30 % in the apparent sediment settling velocity can result in turbulent flows. The model helps explain the particle settling data in previous grid turbulence studies. A relationship for estimating the reduction in settling velocity based on the ratio of RMS turbulent velocity fluctuation to stillwater settling velocity (σ/w_s) is established. Eulerian CFD model predictions of particle-laden jets using such a local correction of particle settling velocity as a function of turbulence intensity are significantly improved as compared to using directly the stillwater settling velocity.

A particle tracking model is developed for horizontal sediment-laden jets. Analytical mean flow solutions and semi-empirical turbulence property (RMS turbulent velocity fluctuations and turbulent dissipation rates) profiles derived from CFD solutions are prescribed in the particle tracking model. Model predictions are in excellent agreement with experimental data of bottom deposition profiles. For the first time the cross-sectional sediment concentration profiles in a horizontal sediment jet are satisfactorily predicted. The model correctly predicts the reduction in sediment settling velocity in a jet due to the turbulence interaction. The particle tracking model is superior to a three-dimensional Eulerian CFD model as it does not require any *a priori* adjustment of the settling velocity.

The present simplified particle tracking model works well for sediment-laden jet with sand and glass particles. Additional studies (not shown) showed that when lighter plastic particles of relative density 1.1 and 1.5 are used, a more general model based on solving the full equation of motion of sediment particles needs to be used to explain the deposition profiles of horizontal sediment-laden jets with a wide range of particle density and sizes. This work will be separately reported.

Acknowledgment This research in supported by a grant from the Hong Kong Research Grants Council (RGC HKU719408) and in part by a grant from the University Grants Committee of Hong Kong (Project No. AoE/P-04/04) to the Area of Excellence (AoE) in Marine Environment Research and Innovative Technology (MERIT).

Appendix 1: Derivation of the particle velocity autocorrelation function

Nielsen [21] has derived the particle velocity autocorrelation function (Eqs. 4 and 9) and the derivation is included here for completeness. The derivation starts with the Lagrangian velocity auto-correlation function

$$R(\Delta t) = \frac{\langle u'(t)u'(t+\Delta t)\rangle}{\sigma^2} \tag{25}$$

where $u'(t)$ is the Lagrangian turbulent fluid velocity fluctuations, and $<>$ denotes the ensemble average. Such correlation function can be modelled by the exponential decay function [29]

$$R(\Delta t) = \exp\left(-\frac{\Delta t}{T_L}\right) \tag{26}$$

By definition,

$$\langle|\Delta u'|\rangle = \left\langle\left|\frac{du'}{dt}\right|\right\rangle \Delta t = \frac{\sigma}{T_L}\Delta t \tag{27}$$

Correspondingly the autocorrelation function may be written as

$$R = \exp\left(-\frac{\langle|\Delta u'|\rangle}{\sigma}\right) \tag{28}$$

Consider the velocity derivative in its Eulerian form

$$\frac{du'}{dt} = \frac{\partial u'}{\partial t} + u'\frac{\partial u'}{\partial x} + v'\frac{\partial u'}{\partial y} + w'\frac{\partial u'}{\partial z}, \tag{29}$$

Equation 27 may be written as

$$\langle|\Delta u'|\rangle = \left\langle\left|\frac{\partial u'}{\partial t} + u'\frac{\partial u'}{\partial x} + v'\frac{\partial u'}{\partial y} + w'\frac{\partial u'}{\partial z}\right|\right\rangle \Delta t \tag{30}$$

To obtain the ensemble average of the Eularian velocity increment, Nielsen [21] has made two assumptions: (1) the loitering effect: the ensemble average depends on the velocity of the previous time step as small velocities correspond to slow changes of velocity, and (2) the cross-correlations between the velocity components (u', v', w') and their partial derivatives $\left(\frac{\partial u'}{\partial t}, u'\frac{\partial u'}{\partial x}, v'\frac{\partial u'}{\partial y}, w'\frac{\partial u'}{\partial z}\right)$ are zero. Thus the ensemble average is written as

$$\langle|\Delta u'|\rangle = \Delta t\sqrt{\left\langle\left(\frac{\partial u'}{\partial t}\right)^2\right\rangle + u_i'^2\left\langle\left(\frac{\partial u'}{\partial x}\right)^2\right\rangle + v_i'^2\left\langle\left(\frac{\partial u'}{\partial y}\right)^2\right\rangle + w_i'^2\left\langle\left(\frac{\partial u'}{\partial z}\right)^2\right\rangle} \tag{31}$$

Applying the Eulerian equivalents to the ensemble values of the partial derivatives

$$\left\langle\left|\frac{\partial u'}{\partial t}\right|\right\rangle = \frac{\sigma}{T_E} \tag{32}$$

and

$$\left\langle\left|\frac{\partial u'}{\partial x}\right|\right\rangle = \left\langle\left|\frac{\partial u'}{\partial y}\right|\right\rangle = \left\langle\left|\frac{\partial u'}{\partial z}\right|\right\rangle = \frac{\sigma}{L_E}, \tag{33}$$

the ensemble average of the Eulerian velocity increment can be derived as

$$\langle|\Delta u'|\rangle = \frac{\sigma\,\Delta t}{T_E}\sqrt{1 + A_E\left[\left(\frac{u_i'}{\sigma}\right)^2 + \left(\frac{v_i'}{\sigma}\right)^2 + \left(\frac{w_i'}{\sigma}\right)^2\right]} \tag{34}$$

with the introduction of

$$A_E = \frac{\sigma T_E}{L_E}. \tag{35}$$

Substitution in Eq. 28 results in the corresponding autocorrelation function:

$$R_i = \exp\left(-\frac{\Delta t}{T_E}\sqrt{1 + A_E\left[\left(\frac{u_i'}{\sigma}\right)^2 + \left(\frac{v_i'}{\sigma}\right)^2 + \left(\frac{w_i'}{\sigma}\right)^2\right]}\right) \tag{36}$$

as in Eq. 4.

For a sediment particle with velocity $\mathbf{u_p}$ defined according to Eq. 1, the particle velocity derivative in its Eulerian form is

$$\frac{dw_p'}{dt} = \frac{\partial w'}{\partial t} + u'\frac{\partial w'}{\partial x} + v'\frac{\partial w'}{\partial y} + (w' - w_s)\frac{\partial w'}{\partial z}, \tag{37}$$

For the simplified particle tracking model which neglects inertia and drag terms, the Lagrangian autocorrelation function for a sediment particle can be similarly shown as in Eq. 9

$$R_i = \exp\left(-\frac{\Delta t}{T_E}\sqrt{1 + A_E\left[\left(\frac{u_i'}{\sigma}\right)^2 + \left(\frac{v_i'}{\sigma}\right)^2 + \left(\frac{w_i' - w_s}{\sigma}\right)^2\right]}\right) \tag{38}$$

Appendix 2: Experimental support of trapping effect in jet turbulence

Nielsen's Lagrangian autocorrelation function for a sediment particle consists of an important assumption that generates the so called 'loitering' effect which results in the reduction of settling velocity—the assumption of "slow velocity corresponds to slow change of velocity". This represents a turbulent structure that when a particle reaches a region of slow velocity, the particle would be trapped with reduced motion as the change of velocity Δw is slow. With this assumption the particle tracking model works well in predicting the deposition of horizontal turbulent sediment laden jets. However, as remarked by Nielsen [21], the assumption has not been proved in any types of flow.

Such an assumption can be supported if it can be shown a positive correlation exists between the velocity magnitude $|u'|$ and the absolute value in the change in velocity $|\partial u'/\partial t|$. We have studied the basis of this assumption using high frequency PIV measurements of turbulent flow velocities of a horizontal jet. The horizontal and vertical velocities of a turbulent jet are measured for two cases $u_0 = 0.392$ and 0.786 m/s in a longitudinal vertical plane using the same experimental set up as described. The time interval of velocity measurement is 5–10 ms which is sufficient to capture the turbulent fluctuations. The correlations between $|u'|$ and $|\partial u'/\partial t|$, and $|w'|$ and $|\partial w'/\partial t|$ are analysed.

From the measurement and the analysis there is a significant correlation between $|w'|$ and $|\partial w'/\partial t|$, from about 0.3 at $x = 30D$ to 0.6 at $x = 50D$ along the jet centerline (Fig. 18). On the other hand the correlation between $|u'|$ and $|\partial u'/\partial t|$ is much less significant. Also, along the shown cross-sections, the correlation of $|w'|$ and $|\partial w'/\partial t|$ is significantly higher. This gives the first direct experimental evidence that the assumption of "slow velocity corresponds to slow change of velocity" is valid in a jet.

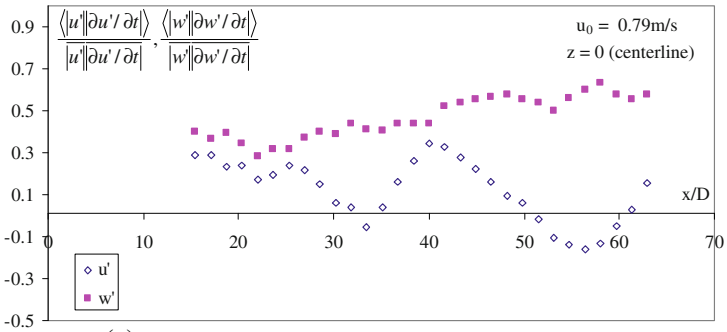

(a) Correlation coefficients along jet centerline

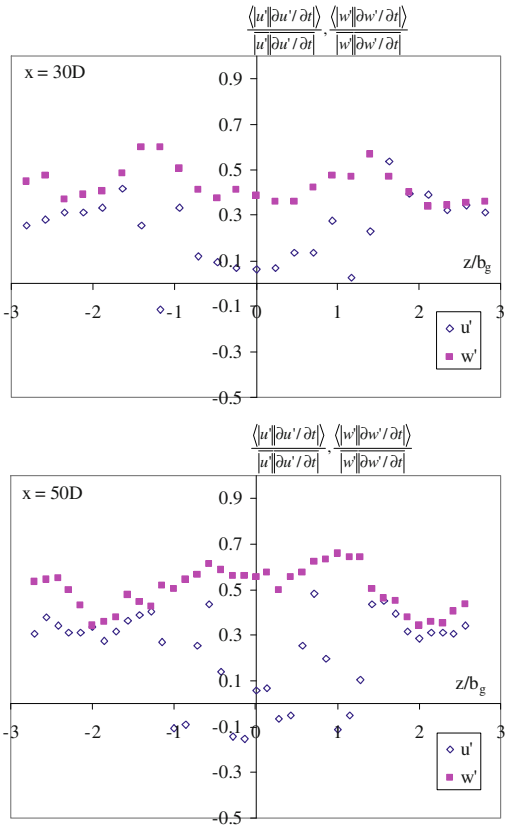

(b) Correlation coefficients along vertical transects at $x = 30D$ and $x = 50D$

Fig. 18 The correlation between $|u'|$ and $|\partial u'/\partial t|$, $|w'|$ and $|\partial w'/\partial t|$, $u_0 = 0.79$ m/s

References

1. Bleninger T, Carmer CV, Jirka G, Neves M (2002) Sedimentation from low concentration particle-laden jets. In: Proceedings of 2nd international conference of marine waste water discharges, 16–20 Sept, Istanbul

2. Cardoso SSS, Zarrebini M (2002) Sedimentation from surface currents generated by particle-laden jets. Chem Eng Sci 57(8):1425–1437
3. Clift R, Grace JR, Weber ME (1978) Bubbles drops and particles. Dover Publications, New York
4. Csanady GT (1963) Turbulent diffusion of heavy particles in the atmosphere. J Atmos Sci 20:201–208
5. Cuthbertson AJS, Apsley DD, Davies PA, Lipari G, Stansby PK (2008) Deposition from particle-laden, plane, turbulent, buoyant jets. J Hydraul Eng ASCE 134(8):1110–1122
6. Doroodchi E, Evans G, Schwarz M, Lane G, Shah N, Nguyen A (2008) Influence of turbulence intensity on particle drag coefficients. Chem Eng J 135:129–134
7. Ernst GGJ, Sparks RSJ, Carey SN, Bursik MI (1996) Sedimentation from turbulent jets and plumes. J Geophys Res B Solid Earth 101(3):5575–5589
8. Fischer HB, List EJ, Koh RCY, Imberger J, Brooks NH (1979) Mixing in inland and coastal waters. Academic Press, New York
9. Ho HW (1964) Fall velocity of a sphere in a field of oscillating fluid. PhD thesis, State University of Iowa
10. Jiang J, Law AWK, Cheng NS (2005) Two-phase analysis of vertical sediment-laden jets. J Eng Mech ASCE 131(3):308–318
11. Kuang CP, Lee JHW (2006) Stability and mixing of a vertical axisymmetric buoyant jet in shallow water. Environ Fluid Mech 6:153–180
12. Lane-Serff GF, Moran TJ (2005) Sedimentation from buoyant jets. J Hydraul Eng ASCE 131(3):166–174
13. Launder BE, Spalding DB (1974) The numerical computation of turbulent flows. Comput Methods Appl Mech Eng 3(2):269–289
14. Lee JHW, Cheung V (1990) Generalized lagrangian model for buoyant jets in current. J Environ Eng ASCE 116(6):1085–1106
15. Lee JHW, Chu VH (2003) Turbulent jets and plumes: a Lagrangian approach. Kluwer Academic Publishers, Boston
16. Lee KWY (2010) Mixing of sediment-laden jet. PhD thesis, The University of Hong Kong, Hong Kong
17. Lee KWY, Li ACY, Lee JHW (2013) Structure of a horizontal sediment-laden momentum jet. J Hydraul Eng ASCE 139(2):124–140
18. Li ACY (2006) Theoretical modeling and experimental studies of particle-laden plumes from wastewater discharges. M.Phil. thesis, The University of Hong Kong, Hong Kong
19. Murray SP (1970) Settling velocities and vertical diffusion of particles in turbulent water. J Geophys Res 75(9):1647–1654
20. Neves MJ, Fernando HJS (1995) Sedimentation of particles from jets discharged by ocean outfalls: a theoretical and laboratory study. Water Sci Technol 32(2):133–139
21. Nielsen P (1992) Coastal bottom boundary layers and sediment transport. Advanced series on ocean engineering, vol 4. World Scientific, Singapore
22. Nielsen P (1993) Turbulence effects on the settling of suspended particles. J Sediment Petrol 63(5):835–838
23. Papanicolaou PN, List EJ (1988) Investigations of round vertical turbulent buoyant jets. J Fluid Mech 195:341–391
24. Parthasarathy RN, Faeth GM (1987) Structure of particle-laden turbulent water jets in still water. Int J Multiph Flow 13(5):699–716
25. Shih TH, Liou WW, Shabbir A, Yang Z, Zhu J (1995) A new k-ϵ eddy viscosity model for high Reynolds number turbulent flows. Comput Fluids 24(3):227–238
26. Singamsetti S (1966) Diffusion of sediment in a submerged jet. J Hydraul Div Proc ASCE 92(2):153–168
27. Soulsby R (1997) Dynamics of marine sands: a manual for practical applications. Thomas Telford, London
28. Sparks RSJ, Carey SN, Sigurdsson H (1991) Sedimentation from gravity currents generated by turbulent plumes. Sedimentology 38(5):839–856
29. Taylor GI (1921) Diffusion by continuous movements. Proc Lond Math Soc 20:196–211
30. Wang H, Law AWK (2002) Second-order integral model for a round turbulent buoyant jet. J Fluid Mech 459:397–428
31. Zhou Q, Cheng NS (2009) Experimental investigation of single particle settling in turbulence generated by oscillating grid. Chem Eng J 149:289–300